ELSEVIER

Journal of Alloys and Compounds 446–447 (2007) 355–359

Journal of ALLOYS AND COMPOUNDS

www.elsevier.com/locate/jallcom

High throughput screening of the ternary $LiNH_2$–MgH_2–$LiBH_4$ phase diagram

G.J. Lewis [a,*], J.W.A. Sachtler [a], J.J. Low [a], D.A. Lesch [a], S.A. Faheem [a], P.M. Dosek [a], L.M. Knight [a], L. Halloran [a], C.M. Jensen [b], Jun Yang [c], Andrea Sudik [c], Donald J. Siegel [c], Christopher Wolverton [c], Vidvuds Ozolins [d], Shu Zhang [e]

[a] *UOP LLC, 25 E. Algonquin Rd, Des Plaines, IL 60017, USA*
[b] *Hawaii Hydrogen Carriers, LLC, Honolulu, HI, USA*
[c] *Ford Motor Company, Research and Advanced Engineering, MD 3083/RIC, Dearborn, MI 48121, USA*
[d] *Department of Materials Science and Engineering, University of California, Los Angeles, CA 90095-1595, USA*
[e] *Department of Chemistry, University of Hawaii, Honolulu, HI 96822, USA*

Received 1 November 2006; received in revised form 1 April 2007; accepted 3 April 2007
Available online 8 April 2007

Abstract

Here we apply combinatorial synthesis and screening (CSS) techniques with synthesis and testing of up to 48 samples in parallel to increase the rate of discovery of improved complex hydrides and dopants. In this paper we will demonstrate the application of CSS to a detailed investigation of the ternary $LiNH_2$–MgH_2–$LiBH_4$ phase diagram. Most points on this phase diagram yield materials with high theoretical hydrogen storage and offer the potential for improved storage properties as inspired by previous studies of binary systems (edges of the phase diagram) that have yielded interesting results in the literature. By using CSS we have found ternary mixtures that exhibit reversible chemistry similar to the $2LiNH_2$–MgH_2 system that have superior properties with respect to reversibility and desorption temperature, an optimum occurring at $0.6LiNH_2$–$0.3MgH_2$–$0.1LiBH_4$. Hydrogen storage capacities and the structural characterization of the as-synthesized and dehydrided materials will be reported as a function of composition. Detailed characterization of the most promising materials will also be presented.

Keywords: Hydrogen absorbing materials; Mechanical alloying; X-ray diffraction; Thermal analysis; Combinatorial chemistry; High throughput characterization

1. Introduction

The search for alteratives to compliment and eventually replace fossil fuels has commenced. Hydrogen is one alternative under consideration, particularly because of its potential for a favorable environmental impact. One of the hurdles to developing hydrogen as an alternative energy carrier is a method for hydrogen storage that provides acceptable gravimetric and volumetric capacity. While the storage of hydrogen in both liquid and gaseous forms is being pursued, each has their disadvantages and complex metal hydrides have emerged as a potential option. A landmark paper by Bogdanovic and Schwickardi [1] showed that Ti-doped $NaAlH_4$ could operate reversibly under 200 °C at reasonable pressures with nearly 5 wt.% reversible hydrogen storage, and has inspired a great deal of interest in complex metal hydrides.

Another hurdle in identifying new hydrogen storage materials is the time it takes to evaluate them. The traditional approach of evaluation uses a pressure–composition–temperature (PCT) apparatus to measure hydrogen desorption and uptake, measurements that can take from a few days to a few weeks. High throughput and combinatorial experimental approaches have been developed in other fields that have greatly accelerated the rate of discovery. The basic elements of the high throughput approach include operating in parallel, applying automation where possible, and the development of an assay that can quickly determine if a sample is promising or not. It has been our goal to develop these methods for the investigation of hydrogen storage materials. We first developed a medium throughput assay which can measure hydrogen capacities for eight samples at a time. The

* Corresponding author. Tel.: +1 847 912 9237; fax: +1 847 391 3219.
E-mail address: gregory.lewis@uop.com (G.J. Lewis).

0925-8388/$ – see front matter © 2007 Elsevier B.V. All rights reserved.
doi:10.1016/j.jallcom.2007.04.028

assay measures the hydrogen evolved as the sample is ramped at 2 °C/min to 220 °C. The samples are rehydrided and another desorption cycle is performed. This non-equilibrium measurement focuses on kinetic aspects of the hydrogen desorption. Promising materials are those that show significant desorption during the second cycle, which is taken to be a measure of the reversible hydrogen. We have extended this approach to a high throughput assay that can measure hydrogen capacities for 48 samples simultaneously. The same multiple desorption–hydriding cycle approach used in the medium throughput system is employed in the high throughput assay, but higher desorption/rehydriding temperatures (up to 350 °C) can be investigated. At this time, the development of high throughput synthesis methods for hydrogen storage materials is still underway.

In this paper, we describe the application of both medium and high throughput methods to the investigation of hydrogen storage compositions derived from the $LiNH_2$–MgH_2–$LiBH_4$ phase diagram, which is shown in Fig. 1. This system is intriguing because some of the binary systems have been investigated in the literature. The $2LiBH_4$–MgH_2 system was investigated by Vajo et al. and found to yield 8–10 wt.% reversible hydrogen at temperatures around 350 °C [2]. The $2LiNH_2$–$LiBH_4$ system was studied by Pinkerton et al. and was found to yield >10 wt.% hydrogen at temperatures greater than 250 °C, but was not reversible and surprisingly yielded the new phase $Li_4BH_4(NH_2)_3$ [3]. The $2LiNH_2$–MgH_2 system was investigated by Xiong et al. [4] and by Luo [5]. This system operates above 200 °C and is reversible, ideally yielding nearly 5.6 wt.% hydrogen. The phase diagram investigated here includes these binary compositions as well as ternary $LiNH_2$–MgH_2–$LiBH_4$ compositions which to our knowledge have not been investigated. Given the richness of the chemistry observed in the binary systems, it seems that the ternary system should be fruitful as well.

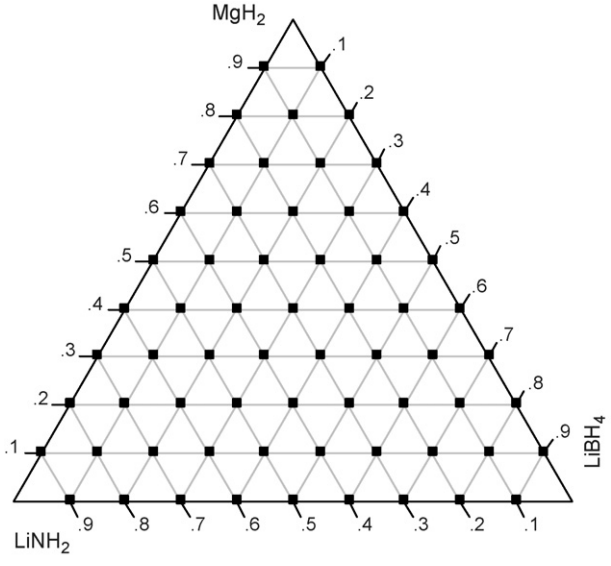

Fig. 1. Phase diagram of $LiNH_2$–MgH_2–$LiBH_4$ compositions studied. The mole fractions $x(LiNH_2) + y(MgH_2) + z(LiBH_4) = 1$ and are varied in 0.1 mol fraction increments.

2. Experimental

Reagents were used as received without further purification. MgH_2 (98%) was purchased from ABCR, while $LiNH_2$ (95%) and $LiBH_4$ (95%) were purchased from Sigma–Aldrich Chemical. All manipulations of samples occurred under an inert nitrogen atmosphere, either in gloveboxes or appropriately sealed vessels. Samples were prepared on a 1 g scale according to the $LiNH_2$–MgH_2–$LiBH_4$ compositions specified in the phase diagram in Fig. 1. Appropriate amounts of each reagent were transferred to 45 ml tungsten carbide milling bowls containing eighteen 10 mm tungsten carbide milling balls. The milling bowls were then sealed from the atmosphere with electrical tape. The samples were placed in a Fritsch Planetary Ball mill, usually 4 at a time, and milled at 350 rpm for an hour, changing the direction of rotation every 15 min. After milling and hydrogen capacity testing, the samples were characterized by high throughput powder X-ray diffraction, using a Bruker-AXS GADDS, system, equipped with an area detector. Measurements were made over a 60-s period, covering a 2θ range of 19.5–54.5° with Cu Kα radiation. More detailed measurements on samples of interest were carried out in an isolation chamber on a Scintag X-1 powder X-ray diffractometer over a 2θ range of 2–90° with Cu Kα radiation.

Medium throughput hydrogen capacity assay was performed in an instrument that can analyze eight samples simultaneously. A 0.5 g portion of sample was loaded into each reactor. Initially, the samples are exposed to 87 bar H_2 at 125 °C for 12 h. Then the first desorption cycle was performed with the pressure due to hydrogen evolution monitored as the samples were ramped at 2 °C/min from room temperature to 220 °C, followed by a 1 h hold at 220 °C. The samples were then rehydrided and run through a second desorption cycle under the same conditions. The hydrogen evolved during the second desorption is reported here as the "reversible" hydrogen. The high throughput hydrogen capacity assay was performed on a proprietary instrument that can analyze 48 samples simultaneously. The hydrogen evolution is measured volumetrically against atmospheric pressure. Desorption cycles can be run up to 350 °C in this instrument. As with the medium throughput unit, multiple desorption and rehydriding cycles were carried out, covering multiple desorption temperatures. In this instrument, the rehydriding pressure was increased to 120 bar H_2. Hydrogen evolution measured during the second desorption cycle was again considered to be "reversible" hydrogen. Temperature programmed reactions with mass spectrometry (TPR/MS) were carried out to detect species like ammonia and diborane that may come off the samples during desorption cycles. The in-house built TPR/MS instrument employed a TCD detector in parallel with a Hiden Analytical RC RGA mass spectrometer. After drying at 120 °C for 3 h and a helium purge, the reactions were conducted in a 5% H_2/Ar stream with a flow rate of 40 cm^3/min with a linear ramp of 2 °C/min to 400 °C.

3. Results and discussion

The $LiNH_2$–MgH_2–$LiBH_4$ compositions were first examined in the medium throughput assay. The hydrogen capacity results from the second desorption, i.e. the reversible hydrogen stored, are shown on a 3D surface fitted to the data points as well as a corresponding contour plot in Fig. 2. The composition with the best capacity was $0.6LiNH_2$–$0.3MgH_2$–$0.1LiBH_4$, which yields 3.4 wt.% H_2 on the second desorption. The observed capacity then drops off rapidly as only four other adjacent compositions have reversible hydrogen capacities above 2 wt.%, as shown in Table 1. All of these are ternary compositions; none of the binary compositions were among the best performers under the conditions employed, including the literature compositions. To understand the nature of the reversible species involved, an XRD study of a composition very close to the best composition, $0.61LiNH_2$–$0.27MgH_2$–$0.12LiBH_4$, was carried out, the results of which are shown in Fig. 3. After milling, MgH_2 and $LiNH_2$ are present, but $LiBH_4$ has disappeared,

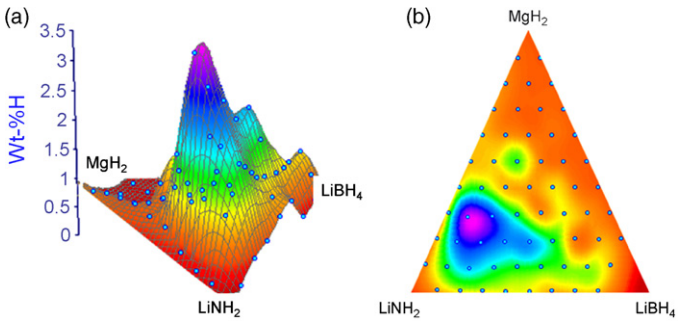

Fig. 2. (a) 3D surface plot and (b) contour plot fitted to the observed reversible hydrogen storage capacity from second desorption to 220 °C for $LiNH_2$–MgH_2–$LiBH_4$ compositions. Highest hydrogen capacity is at $0.6LiNH_2$–$0.3MgH_2$–$0.1LiBH_4$.

Table 1
First and second desorption (2 °C/min ramp to 220 °C) hydrogen capacities for selected phase diagram and optimized (*) compositions

$LiNH_2$	MgH_2	$LiBH_4$	Desorption 1 (wt.% H_2)	Desorption 2 (wt.% H_2)
0.6	0.3	0.1	3.8	3.4
0.5	0.3	0.2	3.5	2.6
0.6	0.2	0.2	2.8	2.6
0.7	0.2	0.1	2.9	2.2
0.5	0.2	0.3	2.7	2.1
0.61	0.27	0.12	3.9	3.4
0.6*	0.3	0.05	4.1	3.8
0.6*	0.3	0.025	4.3	3.6

reacting with $LiNH_2$ to form $Li_4BH_4(NH_2)_3$ (Fig. 3a). In the medium throughput apparatus, the sample was taken through a hydride–desorb–hydride–desorb–hydride program according to the conditions specified above before examination by XRD to determine the species present in the fully hydrided state. The hydrided state of the reversible composition included $Mg(NH_2)_2$, $Li_4BH_4(NH_2)_3$, $Li_2Mg(NH)_2$, and LiH (Fig. 3b). The presence of the mixed imide, $Li_2Mg(NH)_2$, indicates that the hydriding process was incomplete. To examine the dehydrided state, a hydride–desorb cycle was carried out in the high throughput apparatus where the hydrogen is desorbed against atmospheric pressure, whereas the medium throughput apparatus desorbs hydrogen into a constant volume at pressures high enough to prevent complete desorption. The desorption was carried out by ramping to 240 °C at 2 °C/min. The XRD of the resulting material showed $Li_2Mg(NH)_2$ as the major phase, along with some $Li_4BH_4(NH_2)_3$ and Li_3BN_2 (Fig. 3c). These results suggest that the reversible reaction in this system is given by

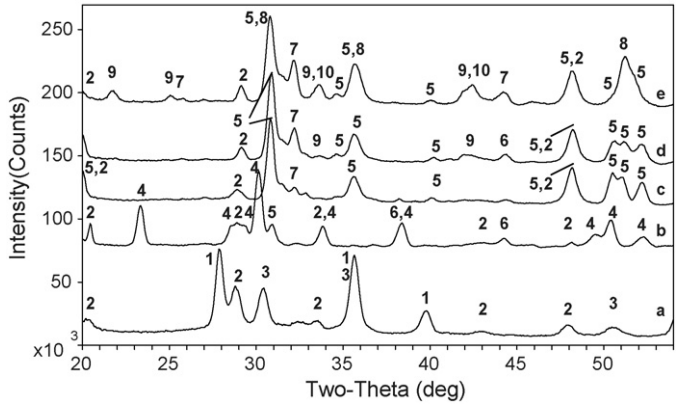

Fig. 3. XRD study of $0.61LiNH_2$–$0.27MgH_2$–$0.12LiBH_4$ composition: (a) after milling, (b) after hydride–desorb–hydride–desorb–hydride cycle, (c) after desorption at 240 °C, (d) after desorption at 300 °C, (e) after desorption at 350 °C. 1, MgH_2; 2, $Li_4BH_4(NH_2)_3$; 3, $LiNH_2$; 4, $Mg(NH_2)_2$; 5, $Li_2Mg(NH)_2$; 6, LiH; 7, Li_3BN_2; 8, "Li_2NH"; 9, Mg_3N_2; 10, MgB_2.

$$Li_2Mg(NH)_2 + 2H_2 \leftrightarrow Mg(NH_2)_2 + 2LiH, \quad (1)$$

which operates in the presence of varying amounts of $Li_4BH_4(NH_2)_3$. The active species are those previously reported for the $2LiNH_2$–MgH_2 system [4,5]. However, while the active species taking part in the hydrogen absorption/desorption reactions in this ternary system are similar to those in the binary $2LiNH_2$–MgH_2 system, the reactivity is much higher. The two compositions in the phase diagram closest to $2LiNH_2$–MgH_2, $0.6LiNH_2$–$0.4MgH_2$ and $0.7LiNH_2$–$0.3MgH_2$, yielded 0.5 and 0.2 wt.% reversible H_2, respectively, considerably less than the 3.4 wt.% observed in the ternary system.

The theoretical hydrogen storage capacity of the $0.6LiNH_2$–$0.3MgH_2$–$0.1LiBH_4$ composition is 11.42 wt.%, much more than accessed in the medium throughput study. The higher temperature hydrogen and stability with respect to decomposition to B_2H_6 and NH_3 were studied by thermal desorption mass spectrometry, shown in Fig. 4. The hydrogen desorption occurs in lower temperature and higher temperature branches, each of which consists of two major peaks. The lower temperature branch shows a major peak at 170 °C and a shoulder at 195 °C. Since desorption is complete by about 225 °C, it is this hydrogen that was characterized by the medium throughput studies above. The higher temperature branch is characterized by desorption peaks at 285 and 300 °C, with hydrogen evolution falling back to the baseline by 350 °C. The mass spectrum shows small ammonia signals (multiplied by a factor of 100 in Fig. 4) at about 100 °C and at 160 and 230 °C, the latter two coincident with the onset of the low and high temperature branches of the hydrogen desorption. The diborane signal (multiplied by a factor of 1000 in Fig. 4) remains in the baseline over the temperature range, suggesting good stability for the boron-containing species.

The phase diagram was then examined in the high throughput apparatus to characterize the higher temperature hydrogen. Using the mass spectrum of the $0.6LiNH_2$–$0.3MgH_2$–$0.1LiBH_4$ composition as a guideline, desorptions were carried out at 220 °C, 285 °C, and twice at 350 °C, with rehydriding steps using 120 bar H_2 at 125 °C in between. The inclusion of the 285 °C desorption step in the program allows access to the lower temperature hydrogen within the higher temperature branch. The results are shown in the contour plots in Fig. 5. The first desorption at 220 °C yields the same best material, $0.6LiNH_2$–$0.3MgH_2$–$0.1LiBH_4$, at 4.8 wt.% H_2 (denoted by X in Fig. 5a). This is higher than observed in the medium throughput apparatus because the hydrogen is desorbed against atmospheric pressure. After rehydriding, the

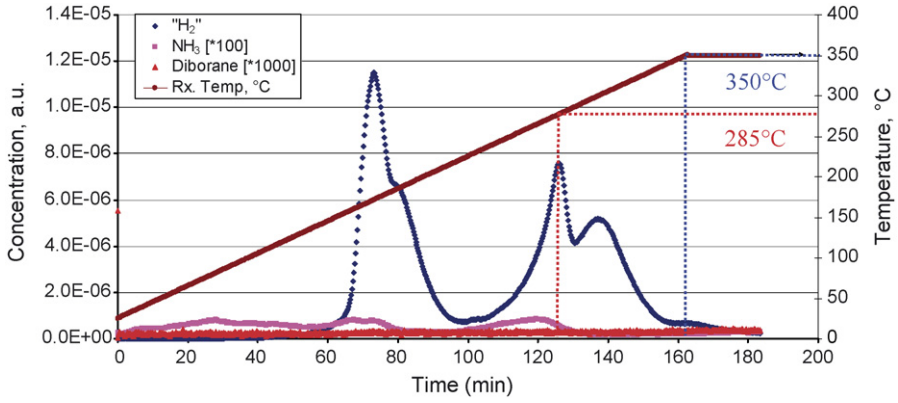

Fig. 4. Thermal desorption mass spectrometry of $0.6LiNH_2$–$0.3MgH_2$–$0.1LiBH_4$ composition showing hydrogen, ammonia, and diborane signals. Ramp rate = 2 °C/min.

second desorption at 285 °C shows the reversible hydrogen for the $0.6LiNH_2$–$0.3MgH_2$–$0.1LiBH_4$ composition and that additionally new hydrogen has been accessed as the desorption has increased to 6.1 wt.% H_2 (denoted by X in Fig. 5b). However, the new maximum desorption compositions are along the $LiNH_2$–$LiBH_4$ binary line as $0.6LiNH_2$–$0.4LiBH_4$ and $0.7LiNH_2$–$0.3LiBH_4$ yield 8.2 and 7.9 wt.% H_2, respectively (denoted by Y and Z in Fig. 5b). Again the samples were hydrided and a third desorption was carried out at 350 °C (not shown in Fig. 5). The compositions showing the best capacity in the previous desorptions were damaged and did not rehydride, all showing drastically reduced capacities of less than 1.5 wt.%. The compositions showing the highest hydrogen capacities approached pure MgH_2, including $0.9MgH_2$–$0.1LiBH_4$, 5.6 wt.%, and $0.8MgH_2$–$0.2LiBH_4$, 5.3 wt.%. These compositions were not active in the lower temperature desorptions. After rehydriding and a fourth desorption at 350 °C, these two compositions again showed the largest but diminished capacities of 3.62 and 4.05 wt.% H_2 (denoted by U and V in Fig. 5c), respectively, perhaps because the hydriding conditions were too mild. Only six other compositions showed desorptions between 1 and 3 wt.% H_2 in this last desorption, indicating that the high temperature desorptions brought about the formation of phases that could not be reversed.

The nature of the irreversible phases was investigated by observing the XRD patterns of dehydrided $0.61LiNH_2$–$0.27MgH_2$–$0.12LiBH_4$ compositions after first desorptions to 300 °C (Fig. 3d) and 350 °C (Fig. 3e). While desorption to 300 °C still shows the formation of reversible $Li_2Mg(NH)_2$, it is apparent that this pattern is partly transforming to a Li_2NH pattern by 350 °C. Progressing from the reversible material isolated after desorption at 240 °C (Fig. 3c) to that isolated after the 350 °C desorption (Fig. 3e), the growing presence of irreversible components such as Li_3BN_2, Mg_3N_2, and MgB_2 is observed.

Since the operable reversible reaction for hydrogen storage in the optimum system appears to be reaction (1) above, we decided to make a direct comparison of the hydrogen desorption properties with the $2LiNH_2$–MgH_2 composition by temperature programmed desorption, shown in Fig. 6. While the lower temperature branch of the hydrogen desorption occurs at 190 °C in the best composition, desorption in the $2LiNH_2$–MgH_2 system is just getting started at this temperature and does not reach a maximum in its low temperature desorption branch until 275 °C. While the operable storage reactions are the same for the two compositions, the reason for the lower temperature desorption in the $0.61LiNH_2$–$0.27MgH_2$–$0.12LiBH_4$ composition must be the presence of $Li_4BH_4(NH_2)_3$, which is present in varying amounts throughout the reversible cycle. This phase was previously reported to melt [3]. The $Li_4BH_4(NH_2)_3$ would be melted at the temperatures over which the reversible hydrogen storage reactions occur in the best material. In the melted state, $Li_4BH_4(NH_2)_3$ can act as a "solvent" to facilitate chemical transport of the species involved in the hydrogen storage reactions in the optimal composition, yielding much lower desorption temperatures than the $2LiNH_2$–MgH_2 system, which relies purely on a solid state reaction.

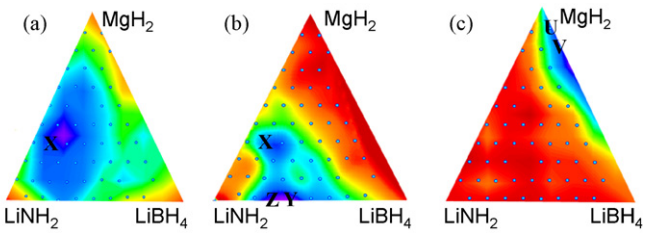

Fig. 5. Hydrogen capacity measurements for the $LiNH_2$–MgH_2–$LiBH_4$ phase diagram using the high throughput apparatus: (a) cycle 1, desorption at 220 °C; (b) cycle 2, desorption at 285 °C; (c) cycle 4, desorption at 350 °C. See text for symbols.

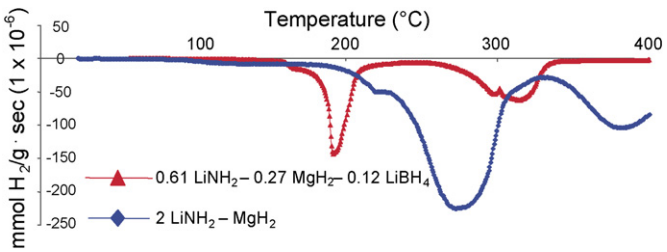

Fig. 6. Comparison of hydrogen desorption properties of $0.61LiNH_2$–$0.27MgH_2$–$0.12LiBH_4$ vs. $2LiNH_2$–MgH_2 via temperature programmed reaction with mass spectrometry (TPR/MS).

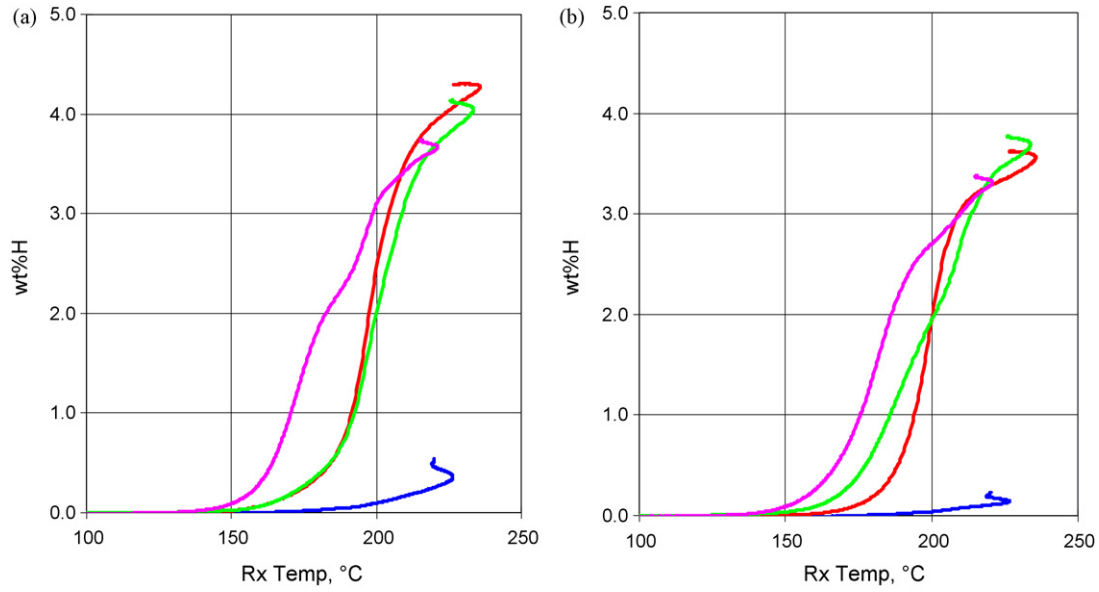

Fig. 7. First (a) and second (b) desorption curves for the $0.6LiNH_2$–$0.3MgH_2$–$xLiBH_4$ series. *Key*: $x = 0.1$, magenta; $x = 0.05$, green; $x = 0.025$, red; $x = 0$, blue.

Taking account of temperature reduction enhancement added by the presence $Li_4BH_4(NH_2)_3$ and the fact that it does not contribute significantly to the hydrogen desorption capacity at temperatures of 220 °C or less, we investigated lower $LiBH_4$ levels of the best phase diagram composition, $0.6LiNH_2$–$0.3MgH_2$–$xLiBH_4$, where $x = 0.05$ and 0.025, to see if the storage capacity could be optimized. The first and second desorption curves for these materials along with those for $2LiNH_2$–MgH_2 ($x = 0$) and the optimum ($x = 0.1$) are shown in Fig. 7. As anticipated, the hydrogen storage capacities are higher (Table 1) for the lower values of x, because there is less of the non-desorbing $Li_4BH_4(NH_2)_3$. However, at the lower $LiBH_4$ levels, desorption becomes more difficult as the temperature shifts upward by about 20 °C. This supports the idea that $Li_4BH_4(NH_2)_3$ does not contribute to the H_2 desorption, but rather serves to facilitate the chemistry in this system, allowing the $2LiNH_2$–MgH_2 system to operate at lower temperatures.

4. Conclusion

An investigation of the $LiNH_2$–MgH_2–$LiBH_4$ phase diagram for new hydrogen storage materials was carried out using combinatorial methods and high throughput techniques. A new family of hydrogen storage materials based on ternary compositions was found, the optimum composition being $0.6LiNH_2$–$0.3MgH_2$–$0.1LiBH_4$. While the actual storage reaction, $Li_2Mg(NH)_2 + 2H_2 \leftrightarrow Mg(NH_2)_2 + 2LiH$, is well known, in this ternary system it operates at lower temperatures due to the presence of $LiBH_4(NH_2)_3$. Over the temperature range at which the hydrogen desorption reactions occur, $Li_4BH_4(NH_2)_3$ is melted and can influence chemical transport properties of the species involved. This leads to the significantly lower hydrogen desorption temperatures observed vs. the $2LiNH_2$–MgH_2 system, which relies solely on a solid-state reaction.

References

[1] B. Bogdanovic, M. Schwickardi, J. Alloys Compd. 253–254 (1997) 1.
[2] J.J. Vajo, S.L. Skeith, F. Mertens, J. Chem. Phys. B 109 (2005) 3719.
[3] (a) G.P. Meisner, M.L. Scullin, M.P. Balogh, F.E. Pinkerton, M.S. Meyer, J. Phys. Chem. B 110 (2006) 4186;
(b) Y.E. Fillinchuk, K. Yvon, G.P. Meisner, F.E. Pinkerton, M.P. Blogh, Inorg. Chem. 45 (2006) 1433.
[4] Z. Xiong, G. Hu, P. Chen, Adv. Mater. 16 (2004) 1522.
[5] W. Luo, J. Alloys Compd. 381 (2004) 284.